processes

MDPI

Article

Highly Dispersed and Stable Ni/SiO_2 Catalysts Prepared by Urea-Assisted Impregnation Method for Reverse Water–Gas Shift Reaction

Ning Liu [1,†], Sha Cui [1,†], Zheyu Jin [2], Zhong Cao [1], Hui Liu [3,*], Shuqing Yang [1], Xianmin Zheng [1] and Luhui Wang [1,4,5,*]

1 Department of Chemical Engineering, School of Petrochemical Technology and Energy Engineering, Zhejiang Ocean University, Zhoushan 316022, China; z20086100074@zjou.edu.cn (N.L.); cuisha2019@zjou.edu.cn (S.C.); s20082000020@zjou.edu.cn (Z.C.); ysqjane@163.com (S.Y.); zheng_xianmin@163.com (X.Z.)
2 Department of Chemical and Biological Engineering, Rensselaer Polytechnic Institute, School of Engineering, Troy, NY 12180, USA; jinz6@rpi.edu
3 School of Food and Pharmaceutical, Zhejiang Ocean University, Zhoushan 316022, China
4 Zhejiang Provincial Key Laboratory of Petrochemical Pollution Control, Zhejiang Ocean University, Zhoushan 316022, China
5 National-Local Joint Engineering Laboratory of Harbor Oil & Gas Storage and Transportation Technology, Zhejiang Ocean University, Zhoushan 316022, China
* Correspondence: liuhui@zjou.edu.cn (H.L.); wangluhui1008@zjou.edu.cn (L.W.)
† These authors contributed equally to this work.

Abstract: The nickel-based catalyst was more active in the reverse water-gas shift reaction, but it is easy to sinter and deactivate in high temperature reaction (≥600 °C). A urea-assisted impregnation method was utilized to create a Ni/SiO_2-N catalyst to increase the catalytic stability of Ni-based catalysts. For at least 20 h, the Ni/SiO_2-N catalyst in the reverse water-gas shift process at 700 °C remained stable, and in the high temperature RWGS reaction, the conversion rate of CO_2 of the catalyst is close to the equilibrium conversion rate. The catalysts were characterized by BET, XRD, H_2-TPR, and TEM, and the results demonstrate that the Ni particles had a small particle size and exhibited strong interaction with the SiO_2 support in the Ni/SiO_2-N catalyst, which led to the catalyst's good activity and stability. Urea-assisted impregnation is a facile method to prepare stable Ni/SiO_2 catalysts with high Ni dispersion.

Keywords: reverse water-gas shift reaction; Ni/SiO_2 catalyst; urea; Ni dispersion; stability

check for updates

Citation: Liu, N.; Cui, S.; Jin, Z.; Cao, Z.; Liu, H.; Yang, S.; Zheng, X.; Wang, L. Highly Dispersed and Stable Ni/SiO_2 Catalysts Prepared by Urea-Assisted Impregnation Method for Reverse Water–Gas Shift Reaction. *Processes* **2023**, *11*, 1353. https://doi.org/10.3390/pr11051353

Academic Editor: Olívia Salomé G.P. Soares

Received: 15 March 2023
Revised: 7 April 2023
Accepted: 25 April 2023
Published: 28 April 2023

1. Introduction

Increased CO_2 emissions in recent years, causing the serious greenhouse effect. At the same time, CO_2 is also the most abundant and cheap C_1 resource. Therefore, the conversion of CO_2 into valuable chemicals and fuels has attracted extensive attention. CO_2 hydrogenation is one of the effective methods to produce a variety of products [1], including CH_4, CO, and C_2H_6O, etc. In different hydrogenation reactions, the reverse water-gas shift (RWGS: $CO_2 + H_2 = CO + H_2O$, $\Delta H = 40.6$ kJ/mol) reaction, which had been thought to be one of the most promising reactions for CO_2 conversion, can transform CO_2 into more valuable CO [2–6]. It can be utilized to perform Fischer-Tropsch synthe-sis in the presence of H_2 to create more valuable compounds.

Nowadays, the research of RWGS reaction catalysts has attracted more and more attention, various catalysts such as copper-based catalysts [7–12], noble metals [13–15], and nickel-based catalysts [16,17] have been used for the study of the reverse water gas shift reaction. Copper-based catalysts have a high selectivity for CO in the RWGS reaction, but their activity is low, and copper particles are easily aggregated during high-temperature reactions. The thermal stability of the copper-based catalyst is poor, and

it quickly deactivates in high-temperature RWGS reactions. However, cop-per-based catalysts' catalytic activity and stability at high temperatures are effectively increased by a little addition of iron [7]. Wang et al. [18] prepared 2D silica ($2DSiO_2$) supported copper catalyst with SMSI. The Cu-$2DSiO_2$ catalyst with unique coated Cu nanoparticles has strong metal-support interaction and shows excellent long-term sta-bility in the RWGS. Kim et al. [13,14] investigated a variety of Pt/TiO_2 catalysts for the RWGS reaction and discovered that the reducibility of the TiO_2 support affects the RWGS activity difference of Pt/TiO_2 catalysts. Tang et al. [19] encapsulated the Ru of 1nm in a hollow SiO_2 shell for RWGS reaction, effectively prevented the sintering of Ru clusters, maintained the excellent activity of Ru in CO_2 hydrogenation reaction, and showed close to 100% CO selectivity and excellent stability at 200–500 °C. Although precious metal catalysts have better RWGS reaction performance, they also have some drawbacks, such as high prices and the potential for producing methane, making it difficult to employ them widely.

Non-noble metal Ni-based catalyst is considered a promising RWGS catalyst [17]. However, it requires a lot of energy to transform chemically stable CO_2 into more reac-tive CO, which requires high temperatures to cleave the C=O chemical bond [20]. There is a problem in that the nickel-based catalyst is usually unstable at high temper-atures [21]. Recently, some researchers have found that stable Ni-based catalysts can be prepared by different methods using urea. Biand et al. [22] reported that the Ni/Al hydrotalcite-like compound catalysts made using the urea hydrolysis approach had better nickel dispersion, smaller nickel particle size, and stronger metal-support con-tact, which improved their capacity to prevent carbon buildup. The Ni dispersion was greater in the Ni/ZrO_2 catalyst produced by the urea combustion method. [23]. In addition, the phase shift from monoclinic ZrO_2 to tetragonal ZrO_2 can be fully completed by urea combustion, and at the same time introduce oxygen vacancies into the lattice of ZrO_2, which is related to the high activity of the catalyst. The NixCo(10-x)/SBA-15 bi-metallic catalyst prepared by Xin et al. [24] using the urea co-precipitation method forms an ordered mesoporous structure. Ni and Co particles were embedded in the pores of SBA-15, and the pore-limiting effect improved the catalyst's stability. The method of urea precipitation (DPU) is considered to be effective for producing highly distributed and stable catalysts, and it was extensively employed in the preparation of monometallic and bimetallic catalysts [25].

SiO_2-supported Ni catalysts have attracted much interest due to the superior character-istics of SiO_2, such as high abundance, easy processability, and low cost [26–28]. However, there are few reports on the preparation of highly dispersed stable Ni/SiO_2 catalysts, there-fore, designing a feasible and low-cost method to prepare highly dispersed stable Ni/SiO_2 catalysts and thereby obtain excellent catalytic activity and stability, especially it is still a challenge at high temperatures.

As far as we know, there are no reports on the preparation of highly stable Ni/SiO_2 catalysts by the urea-assisted impregnation method. Herein, a highly dispersed Ni/SiO_2-N catalyst was prepared using a urea-assisted impregnation method and used for RWGS, which was active and stable in long-term RWGS reaction. Urea as an auxiliary impregnation medium had a significant effect on the metal–support interaction and Ni dispersion.

2. Experiments

2.1. Catalyst Preparation

The urea-assisted incipient wetness impregnation method was used to prepare the Ni/SiO2-N catalyst. In general, 0.496 g $Ni(NO_3)_2{\cdot}6H_2O$ and 1.023 g urea were mixed and 2.85 mL of deionized water was added, followed by ultrasound for 20 min. 1.90 g silica (100–200 mesh, purchased from Qingdao Bangkai High-tech Materials Co., Ltd., Qingdao, China) was added to the above solution and allowed to aforementioned solution, then let it stand for 10 h at room temperature. by drying at 80 °C for 10 h and calcining at 600 °C for 4 h, the Ni/SiO_2-N catalyst was obtained. The same procedure was used to prepare a Ni/SiO_2 catalyst without urea. The theoretical Ni loading of the two catalysts is 5 wt.%.

2.2. Catalyst Characterization

With the Autosorb-iQ analyzer (Quantachrome Instruments (USA), Boynton Beach, FL, USA), N_2 adsorp-tion-desorption isotherms were obtained at a temperature of −196 °C. First, the test tube was weighed to determine its mass (M_1), and then 50 mg catalyst is added. The cata-lyst is then outgassed at a temperature of 300 °C for six hours to remove any impurities. After test, the test tube's mass was measured and recorded as M_2, and the catalyst's mass is calculated as $M = M_2 - M_1$. The Barret-Joyner-Halenda (BJH) method was used to calculate the average pore diameter and pore volume, while the Brunau-er-Emmet-Teller (BET) method was utilized to calculate the specific surface area.

The powder X-ray diffraction (XRD) spectrum of the catalysts were measured us-ing a China Haoyuan Instrument DX-2700 X-ray diffractometer. All catalysts were scanned at 1.2°/min between 10° and 80°. Different crystals' spectral lines correspond to particular positions, quantities, and intensities, respectively. To determine the phase information of the catalyst sample, compare the crystal spectra with the standard PDF card. Then, use the Jade software to reassess the data to determine the catalyst. The Scherrer formula is used to calculate the grain size of the particular phase in the sam-ple based on the specific lattice parameters of the sample. The Equation (1) is as follows

$$D = \frac{K\lambda}{\beta \cos\theta} \tag{1}$$

D is the desired grain size; the K value is a constant related to the crystal size (generally 0.89); λ is the wavelength of the incident X-ray (λ = 0.15 nm); β is the maxi-mum value of the diffraction peak intensity 1/2 peak width; θ is the size of the diffrac-tion angle.

The H_2 temperature-programmed reduction (H_2-TPR) experiment was performed using the TP-5080 instrument with a thermal conductivity detector (TCD). First, 50 mg catalyst was pre-treated with Ar at 400 °C for 30 min and then cooled to room temperature. After that, 5%H_2/Ar gas was introduced for 20 min, and the catalyst was heated from room temperature to 900 °C at a ramp rate of 10 °C/min. The signal of H_2-TPR was detected using a TCD detector.

The Ni dispersion was measured using the TP-5080 instrument through the N_2O titration test. The catalyst of 50 mg was first pretreated with Ar gas at 400 °C for 10 min. After cooling down to room temperature, it was then exposed to 5% H_2/Ar gas and heated from room temperature to 700 °C at a rate of 10 °C/min and kept at 700 °C for 40 min. The TCD detector was used to detect the signal, and S_1 was used to represent the reduction peak area of this process. After cooling the catalyst down to 90 °C, pure N_2O gas was introduced for 30 min, and then the catalyst was cooled down to room temperature before exposing it again to 5% H_2/Ar gas. It was then heated from room temperature to 700 °C at a rate of 10 °C/min for reduction. The TCD detector was used to detect the signal, and S_2 was used to represent the reduction peak area of this process. The dispersion of Ni in the sample could be calculated as $D = S_2/S_1$.

Tecnai G2 F20 microscope was used to characterize the catalyst at 200 kV accel-erating voltage, and transmission electron microscope (TEM) images were formed. Firstly, the catalysts were ultrasonically treated for 30min, then it was evenly dis-persed in acetone, and the mixture of powder and acetone was dripped into copper mesh by capillary tube, and then it was dried and analyzed.

2.3. Catalytic Test

Under the atmospheric pressure, 10 mg catalyst mixed with 100 mg quartz sand were put into a quartz tube fixed bed reactor (Φ = 8 mm). Before the RWGS reaction, the H_2/N_2 = 1/4 mixed gas was heated to 700 °C for reduction for 40 min at a rate of 10 °C/min.

The RWGS reaction was fed with 100 mL/min of H_2/CO_2 gas flow at a feed ratio of 1:1, the space velocity was 6×10^5 mL/g_{cat}/h. and the test temperature range is 400–750 °C. Every temperature point was set at 50 °C, and each one was examined for an hour to get

the average value. Under the same feed conditions, the catalyst was tested for long-term high temperature stability. The components of raw material gas and tail gas were analyzed online on the gas chromatography SP3420A equipped with a TCD detector. The CO_2 conversion and selectivity of the catalyst were calculated by Equations (2)–(4) to evaluate the catalyst

$$X_{CO_2}(\%)conversion = \frac{CO_{2\ in} - CO_{2\ out}}{CO_{2\ in}} \times 100 \quad (2)$$

$$S_{CO}(\%)selectivity = \frac{CO_{out}}{CO_{2\ in} - CO_{2\ out}} \times 100 \quad (3)$$

$$S_{CH_4}(\%)selectivity = \frac{CH_{4\ out}}{CO_{2\ in} - CO_{2\ out}} \times 100 \quad (4)$$

where $CO_{2\ in}$ is the flow rate of CO_2 in the feed gas; $CO_{2\ out}$, CO_{out} and $CH_{4\ out}$ are the flows of CO_2, CO and CH_4 in the exit airflow, respectively.

3. Results and Discussion

The structural characteristics of Ni/SiO_2 and Ni/SiO_2-N catalysts and SiO_2 supports were studied by N_2 adsorption-desorption experiments. As shown in Figure 1a, all samples exhibited Type IV isotherms with H2-type hysteresis loops (IUPAC classification) at relative pressures (P/P_0) ranging from 0.7 to 1.0, indicating the existence of mesoporous structures in the samples [29]. Figure 1b shows that the pore size distribution of all samples is around 10 nm, implying that the original mesoporous structure of the SiO_2 support was well maintained.

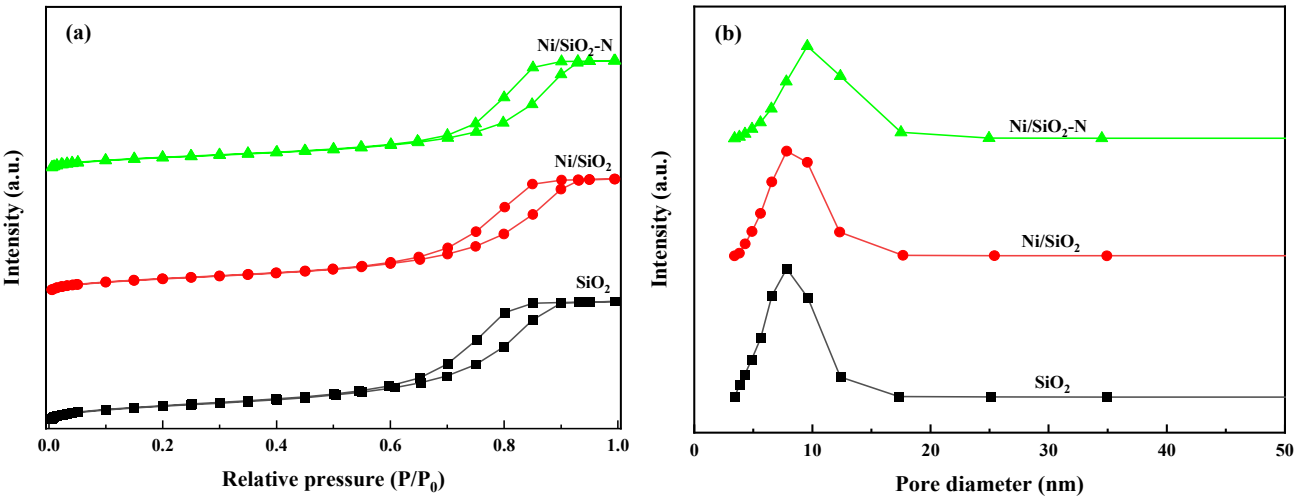

Figure 1. (**a**) Adsorption-desorption of N_2-isotherms, (**b**) Pore size distribution curves.

Table 1 provides a list of the catalysts' specific surface areas (S_{BET}). The SiO_2 support possesses the largest surface area (S_{BET} = 367.4 m^2/g). As expected, the specific surface area of both Ni/SiO_2 and Ni/SiO_2-N catalysts decreased after the addition of NiO, and they are 323.3 m^2/g and 329.6 m^2/g respectively, which was due to some NiO species being located in the pores of SiO_2 or at the entrance of the pores. Moreover, the surface area and average pore size of Ni/SiO_2 and Ni/SiO_2-N were similar. The results show that the structural characteristics of the SiO_2 support are unaffected by the addition of urea.

Table 1. Structural characteristics of Ni/SiO_2 and Ni/SiO_2-N catalysts.

Catalysts	S_{BET} (m^2/g)	Pore Volume (cm^3/g)	Average Pore Size (nm)	d_{NiO} [a] (nm)	d_{Ni} (nm)	
					By XRD	By TEM
SiO_2	367.4	0.9	9.8	-	-	-
Ni/SiO_2	323.3	0.87	10.2	9.7	11.9 [b] (34.8) [c]	14.3 [b] (37.5) [c]
Ni/SiO_2-N	329.6	0.81	10.0	/ [d]	/ [d]	3.8 [b] (4.6) [c]

[a] Calculated by the Scherrer formula from XRD measurements. [b] Ni size of the reduced catalyst. [c] Ni size of the used catalyst. [d] Not calculated due to the weak peak in XRD pattern.

The Ni/SiO_2 and Ni/SiO_2-N catalysts' XRD patterns are shown in Figure 2. Figure 2a shows the fresh catalysts. Figure 2b shows the catalysts were reduced by 50 mL/min of 20% H_2/N_2 mixture at 700 °C for 40 min. All samples have diffraction peaks of amorphous SiO_2 at 2θ = 21.6° [30].

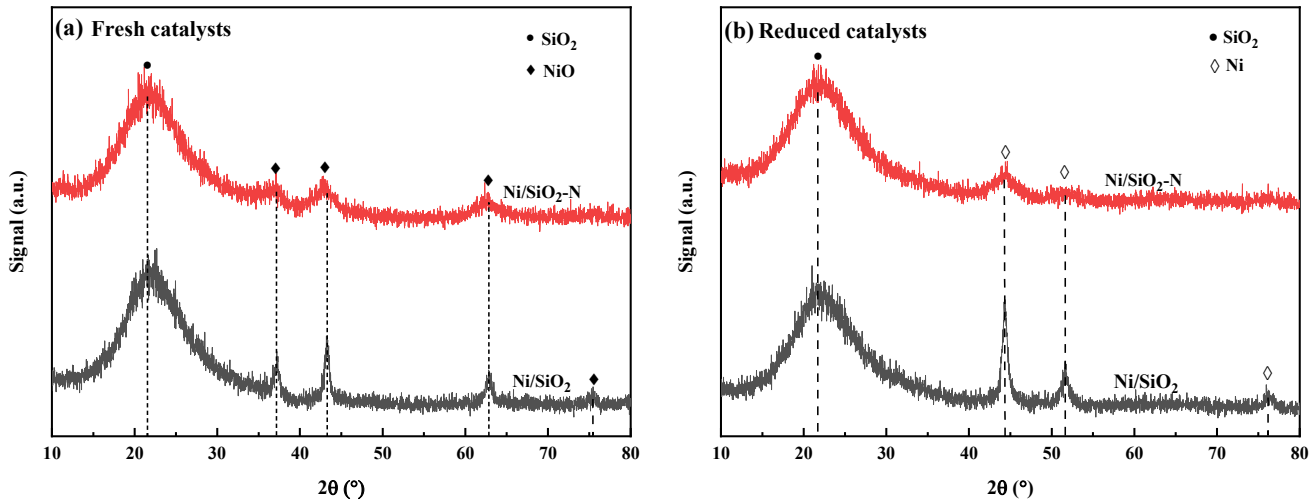

Figure 2. X-ray diffraction (XRD) patterns of (**a**) fresh catalysts, and (**b**) reduced catalysts.

As shown in Figure 2a, the diffraction peaks at 2θ of 37.2°, 43.3°, and 62.9° were observed in the fresh Ni/SiO_2 and Ni/SiO_2-N catalysts, and they were attributed to the (111), (200), and (220) crystal planes of NiO, respectively. The X-ray diffraction pattern of reduced Ni/SiO_2 shows obvious characteristic peaks of metallic Ni, which indicates that larger Ni particles are formed in the catalyst, and the size of metal Ni particles in the Ni/SiO_2 catalyst is 11.9 nm (Table 1), according to the Scherrer formula. Whereas the reduced Ni/SiO_2-N catalyst has weak diffraction peaks of metallic Ni, and the reduced Ni/SiO_2-N catalyst has no diffraction peak at 2θ = 75.45, which means that most metallic Ni in Ni/SiO_2-N catalyst is highly dispersed on the surface of SiO_2 or combined with SiO_2 [31]. The XRD results demonstrate that the addition of urea is conducive to the formation of highly dispersed small particles of Ni-based catalyst.

The H_2-TPR patterns of Ni/SiO_2 and Ni/SiO_2-N catalysts are shown in Figure 3. There are two reduction peaks for the Ni/SiO_2 catalyst. The first reduction peak is about 408 °C(α1), which is similar to the reduction temperature of pure NiO (about 403 °C) reported in the literature and corresponds to the reduction of free NiO [17,32–34]. The second reduction peak is at 428 °C(α2), which is higher than the reduction temperature of pure NiO and can be attributed to the reduction of NiO with weak interaction with SiO_2 [30]. The results indicate that in Ni/SiO_2 catalyst, the interaction between large particles of NiO and SiO_2 support is weak or not at all. The Ni/SiO_2-N catalyst contains a smaller α_2 reduction peak and a larger β reduction peak. The H_2 consumption of the α_2 reduction peak is 108 μmol/g_{cat}, and that of the β reduction peak is 315 μmol/g_{cat}. Reduction at

665 °C Peak β, indicating that the nickel-based species has a strong interaction with the support [35]. The free NiO and some NiO particles with weak interaction with SiO_2 were transformed into highly dispersed NiO particles with strong interaction with the support It may be attributed to the hydrolysis reaction ($CO(NH_2)_2 + H_2O \rightarrow 2NH_3 + CO_2$) in the urea-assisted impregnation process, and the $[Ni(NH)_3)_6]^{2+}$ complex formed by ammonia and Ni can avoid $Ni(OH)_2$ precipitation during impregnation, which is beneficial to the uniform dispersion of Ni species on the surface of SiO_2. At the same time, the alkaline environment formed by urea can slightly dissolve the surface of silica and promote the strong interaction between Ni species and SiO_2 during the calcination process [36].

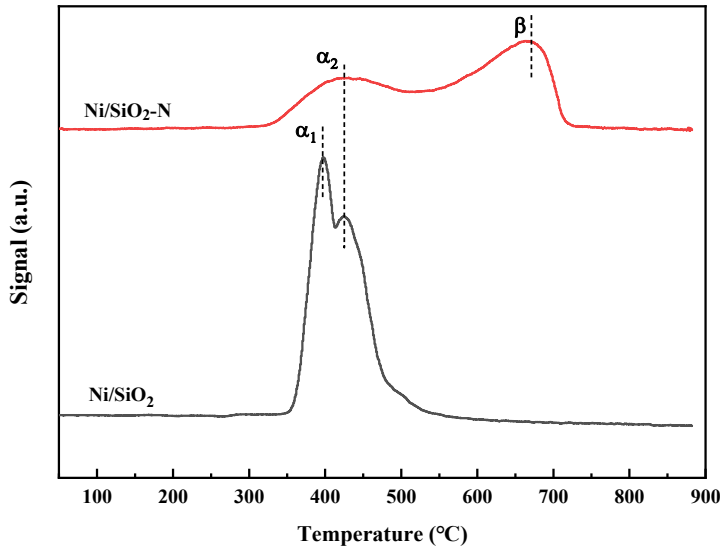

Figure 3. H_2-TPR patterns of fresh Ni/SiO_2 and Ni/SiO_2-N catalysts.

The results of the TEM images of the reduced Ni/SiO_2 and Ni/SiO_2-N catalysts, which were used to investigate the dispersion and determine the particle size of Ni, are shown in Figure 4. For the reduced Ni/SiO_2 catalysts (Figure 4a–c), the Ni metal particles show obvious agglomeration, showing poor Ni dispersion. The particle size distribution diagram is shown in Figure 4b, and its distribution ranges from 6 to 24 nm, with a 14.3 nm particle size on average. The representative region in Figure 4b is extended to form the image of Figure 4c, and a lattice distance of 0.203 nm is observed, which is assigned to Ni(111), indicating the full crystal structure of Ni nanoparticles has been formed. In contrast, for the Ni/SiO_2-N catalyst after H_2 reduction (Figure 4d–f), the metallic Ni particles are uniformly dispersed on the SiO_2 support (Figure 4e), and the particle size distribution of metallic Ni ranges from 2 to 6 nm, with 3.8 nm Ni particles on average. Similarly, as shown in Figure 4f, a lattice spacing of 0.203 nm in length can be observed, ascribed to Ni(111). The results show that the Ni/SiO_2-N prepared by the urea-assisted impregnation method can effectively inhibit the agglomeration of Ni nanoparticles during the high-temperature reduction process, and formed highly dispersed Ni particles with strong interaction with the SiO_2 support, which is consistent with the results of XRD and H_2-TPR.

The Ni dispersion was measured through the N_2O titration test. and the results are listed in Table 2. The dispersions of Ni/SiO_2 and Ni/SiO_2-N catalysts were 7.7% and 24.7%, respectively. According to the particle size in Figure 4b,e, the dispersion of Ni/SiO_2 and Ni/SiO_2-N catalysts was calculated to be 7.1% and 26.6%, respectively, which is close to that of the N_2O titration test. As a result, there are a lot of active sites available for the RWGS reaction and the Ni dispersion can be improved with the addition of urea.

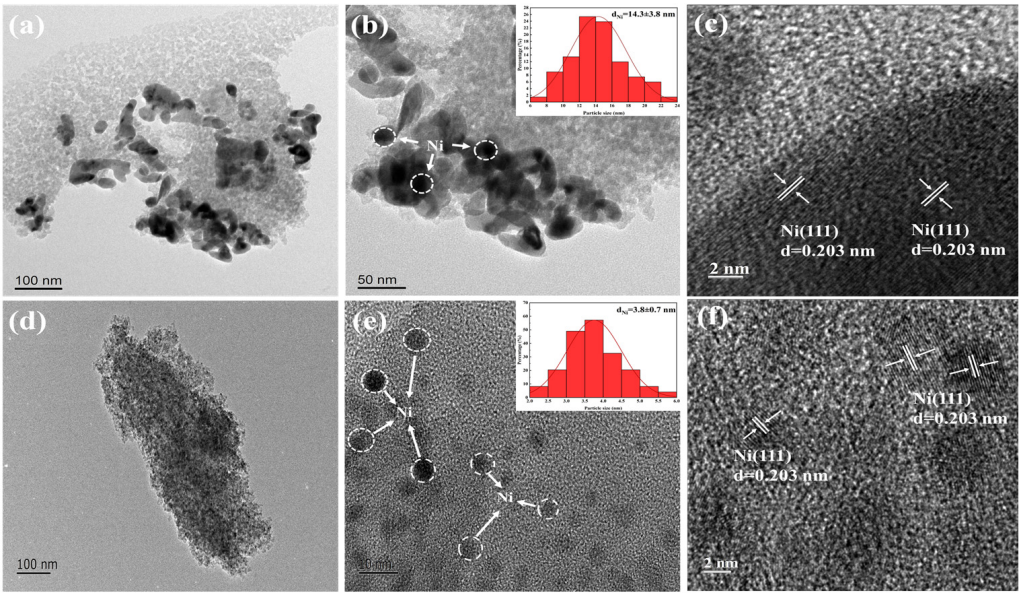

Figure 4. TEM images of the reduced samples. (**a**–**c**) Ni/SiO_2, (**d**–**f**) Ni/SiO_2-N.

Table 2. Metal Dispersion of Ni/SiO_2 and Ni/SiO_2-N catalysts.

Catalysts	D_{Ni} [a] (%)	D_{Ni} [b] (%)
Ni/SiO_2	7.7	7.1
Ni/SiO_2-N	24.7	26.6

[a] Obtained by N_2O titration test. [b] Determined by the expression, $D_{Ni} = 101/d_{Ni}$ (%). The d_{Ni} was measured by TEM as shown in Table 1.

4. Catalytic Performance Test

4.1. Catalyst Performance Test at Different Temperature

Figure 5 shows the RWGS performance tests of catalysts at 400 °C to 750 °C. including (a) CO_2 conversion and (b) selectivity of CO and CH_4. The catalyst's CO_2 equilibrium conversion significantly increased as the reaction temperature increased, whereas the selectivity of CH_4 gradually dropped. This is because the reaction of methanation is an exothermic one that benefits from low temperatures, whereas the reverse water gas shift reaction is an endothermic reaction and benefits more from high temperatures [37]. The only by-product of the Ni/SiO_2 and Ni/SiO_2-N catalysts is CH_4. At the same temperature, the Ni/SiO_2-N catalyst has a higher CO_2 conversion than the Ni/SiO_2 catalyst. Especially, the CO_2 conversion of the Ni/SiO_2 catalyst decreases gradually at the temperatures higher than 600 °C. because during the high temperature reaction process, the Ni particles in the Ni/SiO_2 catalysis have an agglomeration effect, and the metal surface area becomes smaller, which leads to a decrease in the CO_2 conversion of the catalyst, indicating the Ni/SiO_2 catalyst was instable at high temperature. However, the difference is that with the rising temperature, Ni/SiO_2-N's CO_2 conversion rate gradually rises and becomes closer to the equilibrium conversion rate, and the selectivity for CO is close to 100%. Due to the highly dispersed NiO in the Ni/SiO_2-N catalyst has a strong interaction with the SiO_2 support, the Ni nanoparticles are not easy to agglomerate and sinter at high temperature, and the higher CO_2 conversion of Ni/SiO_2-N is related to highly dispersed Ni in the catalyst [17]. According to the characterization results, most of the Ni in Ni/SiO_2-N catalyst is widely scattered on the SiO_2 support and forms small Ni nanoparticles, which provide rich active centers for RWGS reaction and are directly connected to the high activity of the catalyst.

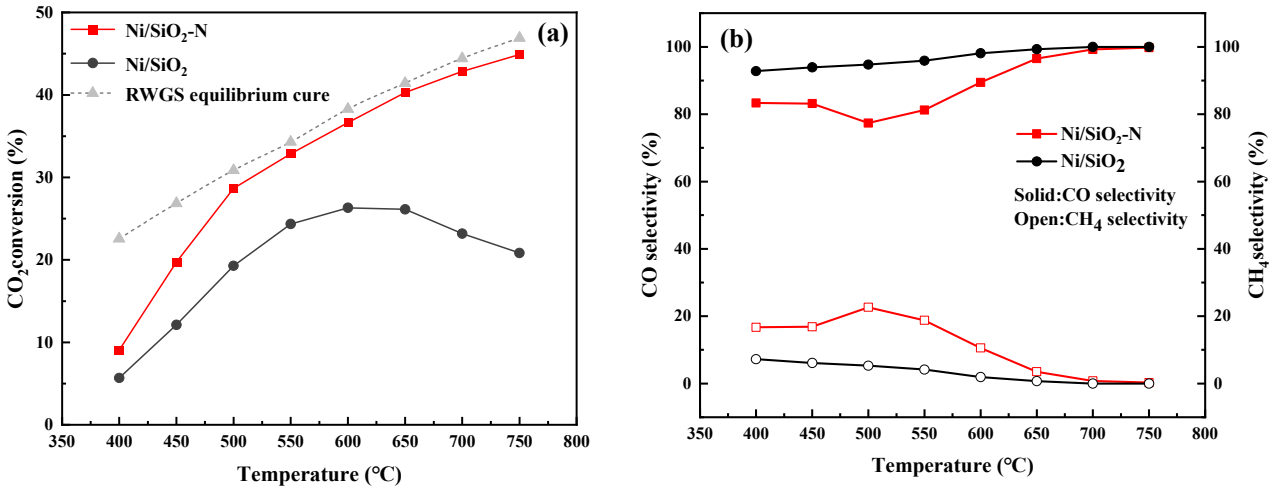

Figure 5. (**a**) CO_2 conversion and (**b**) selectivity of Ni/SiO_2 and Ni/SiO_2-N catalysts.

4.2. Catalyst Stability Test at High temperature

Under high temperature reaction circumstances, the stability of the catalysts is a significant concern for reverse water gas shift catalysts. To assess the stability of the catalysts, a long-term reaction test was performed at 700 °C, and the findings are shown in Figure 6. Under the condition of high temperature, the exothermic methanation reaction is inhibited, so the CO selectivity of both catalysts is close to 100%.

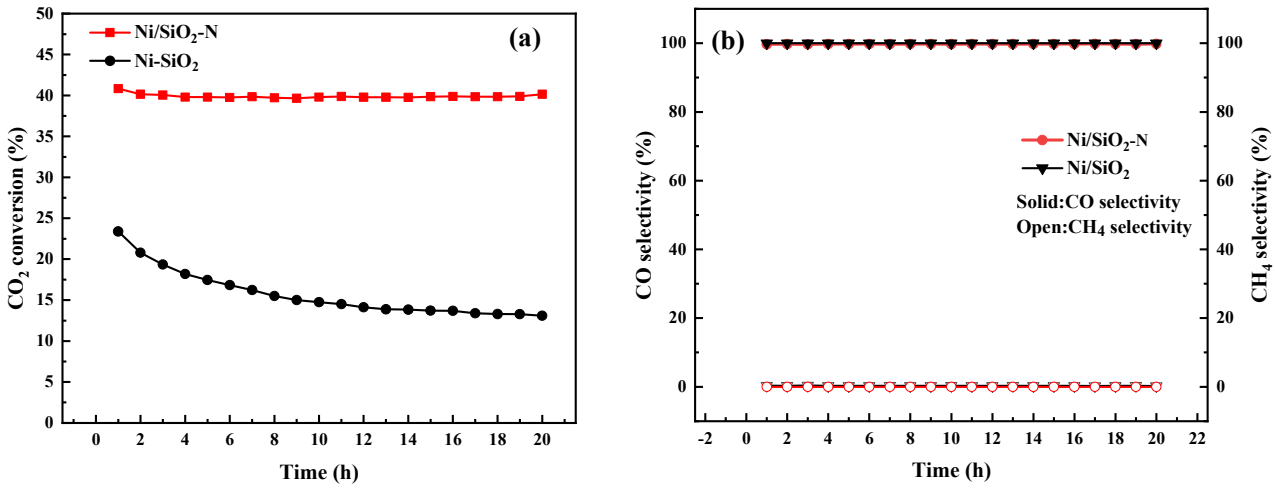

Figure 6. Stability test for Ni/SiO_2 and Ni/SiO_2-N catalysts at 700 °C. (**a**) CO_2 conversion, (**b**) selectivity.

During 20 h reaction process, the CO_2 conversion rate of the Ni/SiO_2 catalyst gradually decreased from 23.4% to 13.1%, and the catalyst only kept 56% of its initial activity. The deactivation rate was 0.022 h^{-1}, which may be caused by the agglomeration and sintering deactivation of large Ni metal during the reaction. On the contrary, the CO_2 conversion rate of the Ni/SiO_2-N catalyst decreased from 40.8% to 40.2%, and the catalyst kept its initial activity of 98.5%. According to the H_2-TPR characterization, it can be known that the using of urea makes the NiO species in the Ni/SiO_2-N catalyst interact strongly with the support SiO_2, effectively avoiding the agglomeration and sintering of Ni species at high temperatures while retaining Ni's high degree of dispersion. Therefore, the Ni/SiO_2-N catalyst demonstrates excellent stability in high temperature reaction tests.

After the RWGS reaction was conducted at 700 °C for 20 h, the catalyst's XRD pattern is shown in Figure 7. The used Ni/SiO_2 catalyst showed the obvious characteristic peak of metallic Ni, according to the Scherrer formula, the Ni size of the used Ni/SiO_2 increased to

34.8 nm (Table 1), indicating that the Ni/SiO_2 catalyst is unstable during the long-term high temperature RWGS reaction, and the Ni particles have an aggregation effect during the reaction process, forming larger metal Ni particles. On the contrary, in the used Ni/SiO_2-N catalyst, the weak Ni diffraction peaks were obtained, and the intensity of the diffraction peak has no obvious change, which demonstrated that the high dispersion and small Ni particle size in the catalyst of Ni/SiO_2-N after a long-term reaction.

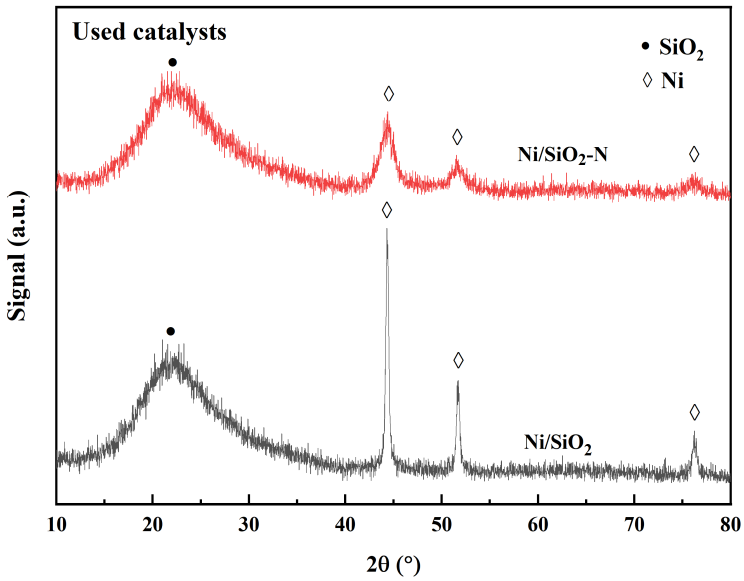

Figure 7. X-ray diffraction (XRD) patterns of catalysts.

Figure 8 shows the TEM images of Ni/SiO_2 and Ni/SiO_2-N catalysts following the stability test. Ni/SiO_2 has an average particle size of 37.5 nm, as evidenced by the particle size statistics in Figure 8b, and large particles of metal Ni were formed, which is much larger than 14.3 nm before the stability test, indicating that the Ni particles are severely agglomerated. On the contrary, after the stability test, the metallic Ni nanoparticles in the Ni/SiO_2-N catalyst highly dispersed on SiO_2 support, which range in size from 3.0 to 6.5 nm, with just 4.6 nm being the average size. The findings indicate that the addition of urea effectively inhibits the sintering of Ni nanoparticles in high temperature reaction, due to the powerful interaction between highly dispersed Ni particles and SiO_2 support. The stability of the catalyst structure is significantly influenced by the addition of urea.

In order to further study the long-term high-temperature reaction stability of the Ni/SiO_2-N catalyst, under the same high temperature test conditions, the catalyst was tested for 50 h of stability. As shown in Figure 9, after the long-term reaction test, CO_2 conversion of the Ni/SiO_2-N catalyst dropped from 40.2% to 39.1%, and the catalyst maintained 97.2% of the initial activity. The deactivation rate of the Ni/SiO_2-N catalyst was 0.00056 h^{-1}, which was only 2.5% of that of the Ni/SiO_2 catalyst (0.022 h^{-1}). The results showed that the stability of the Ni/SiO_2-N catalyst was excellent during 50 h in a high-temperature RWGS reaction.

The catalyst stability test showed that the addition of urea has a substantial effect on the Ni/SiO_2 catalyst's stability. Because of the addition of urea, the catalyst was in the form of Ni metal particles with high dispersion and small particle size, which interact strongly with the SiO_2 support. Therefore, Ni/SiO_2-N catalyst has better thermal stability.

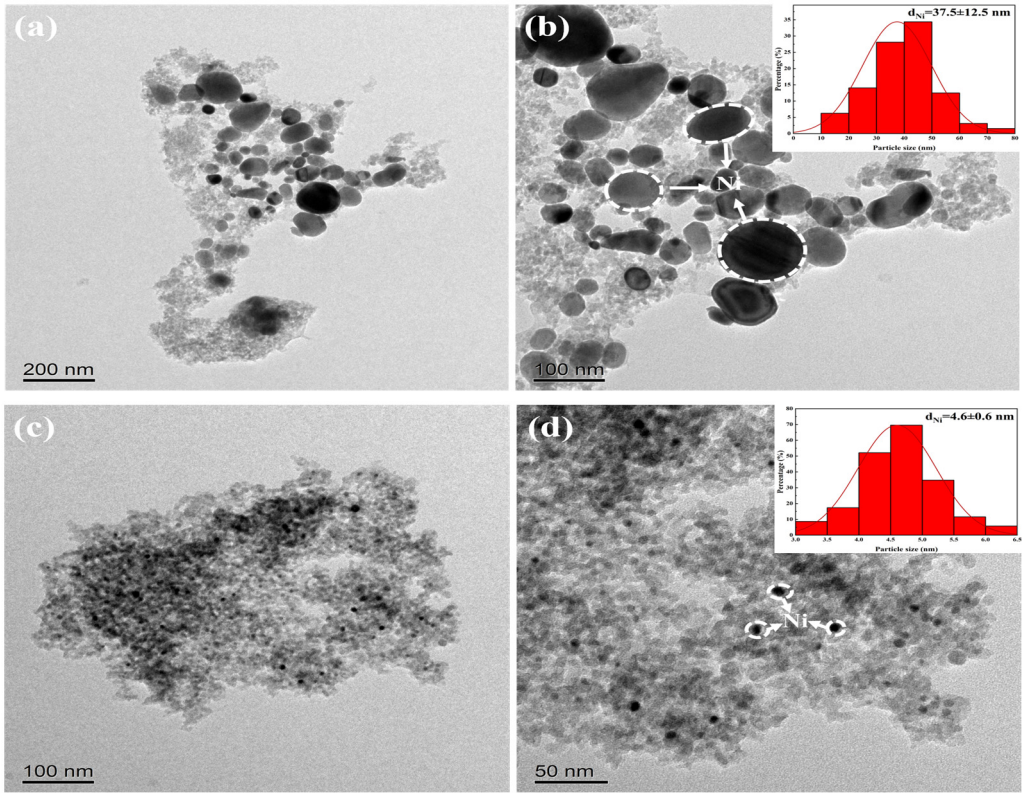

Figure 8. TEM images of the catalysts after the stability test and the size distribution of Ni nanoparticles (**a**,**b**) Ni/SiO_2, (**c**,**d**) Ni/SiO_2-N.

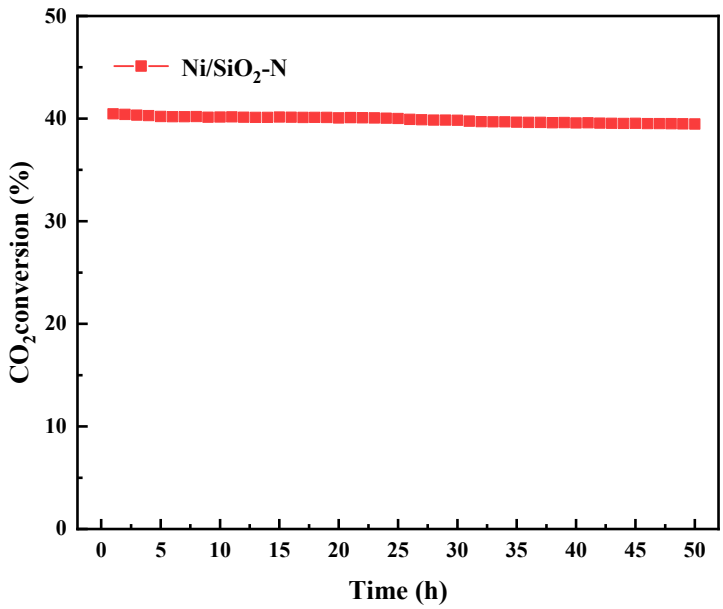

Figure 9. Long-term reaction stability test of Ni/SiO_2-N catalyst at 700 °C.

5. Conclusions

In this study, the Ni/SiO_2-N was prepared using a urea-assisted impregnation method and applied to the RWGS reaction. The Ni/SiO_2 catalyst prepared by the conventional impregnation method, after high temperature reduction, the particle size of Ni reaches 14.3 nm, and its dispersion is only 7.1%, and the catalyst agglomerates and effects during the high temperature reaction, resulting in a decrease in the activity of the catalyst. However, in the process of pre-paring the catalyst, adding urea to the mixture can effectively reduce

the particle size of the active metal Ni, enhance the dispersion of the active metal Ni, and the Ni dispersion can reach 26.6%, improving the interaction between the metal and the SiO_2 support. In addition, in the high temperature RWGS reaction, the conversion rate of CO_2 is close to equilibrium, especially during the long-term high temperature reaction process, the Ni nanoparticles remain highly dispersed and stable, and no active metal agglomeration and sintering effect occurs. This finding highlights the effectiveness of the urea-assisted impregnation method and may inspire the preparation of Ni-based catalysts for high-temperature reactions.

Author Contributions: Conceptualization, L.W.; Investigation, N.L.; Writing—original draft, N.L.; Writing—review and editing, S.C., Z.J., Z.C., H.L., S.Y., X.Z. and L.W.; Project administration, L.W.; Funding acquisition, L.W. All authors have read and agreed to the published version of the manuscript.

Funding: This research was funded by the Science and Technology Foundation of Zhoushan (No. 2022C41002) and the Open Research Subject of Zhejiang Key Laboratory of Petrochemical Environmental Pollution Control (No. 2021Z01).

Data Availability Statement: Data sharing is not applicable to this article.

Conflicts of Interest: The authors declare no conflict of interest.

References

1. Shao, S.; Cui, C.-H.; Tang, Z.; Li, G. Recent advances in metal-organic frameworks for catalytic CO2 hydrogenation to diverse products. *Nano Res.* **2022**, *15*, 10110–10133. [CrossRef]
2. Belekar, R.M. Suppression of coke formation during reverse water-gas shift reaction for CO_2 conversion using highly active Ni/Al_2O_3-CeO_2 catalyst material. *Phys. Lett. A* **2021**, *395*, 127206. [CrossRef]
3. Xu, X.; Moulijn, J.A. Mitigation of CO_2 by Chemical Conversion: Plausible Chemical Reactions and Promising Products. *Energy Fuels* **1996**, *10*, 305–325. [CrossRef]
4. Daza, Y.A.; Kuhn, J.N. CO_2 conversion by reverse water gas shift catalysis: Comparison of catalysts, mechanisms and their consequences for CO_2 conversion to liquid fuels. *RSC Adv.* **2016**, *6*, 49675–49691. [CrossRef]
5. González-Castaño, M.; Dorneanu, B.; Arellano-Garcia, H. The reverse water gas shift reaction: A process systems engineering perspective. *React. Chem. Eng.* **2021**, *6*, 954–976. [CrossRef]
6. Su, X.; Yang, X.; Zhao, B.; Huang, Y. Designing of highly selective and high-temperature endurable RWGS heterogeneous catalysts: Recent advances and the future directions. *J. Energy Chem.* **2017**, *26*, 854–867. [CrossRef]
7. Chen, C.-S.; Cheng, W.H.; Lin, S.S. Enhanced activity and stability of a Cu/SiO_2 catalyst for the reverse water gas shift reaction by an iron promoter. *Chem. Commun.* **2001**, *18*, 1770–1771. [CrossRef]
8. Chen, C.-S.; Cheng, W.-H. Study on the Mechanism of CO Formation in Reverse Water Gas Shift Reaction Over Cu/SiO_2 Catalyst by Pulse Reaction, TPD and TPR. *Catal. Lett.* **2002**, *83*, 121–126. [CrossRef]
9. Chen, C.-S.; Cheng, W.-H.; Lin, S.-S. Study of reverse water gas shift reaction by TPD, TPR and CO_2 hydrogenation over potassium-promoted Cu/SiO_2 catalyst. *Appl. Catal. A Gen.* **2003**, *238*, 55–67. [CrossRef]
10. Chen, C.-S.; Cheng, W.-H.; Lin, S.-S. Study of iron-promoted Cu/SiO_2 catalyst on high temperature reverse water gas shift reaction. *Appl. Catal. A Gen.* **2004**, *257*, 97–106. [CrossRef]
11. Stone, F.S.; Waller, D. Cu–ZnO and Cu–ZnO/Al_2O_3 Catalysts for the Reverse Water-Gas Shift Reaction. The Effect of the Cu/Zn Ratio on Precursor Characteristics and on the Activity of the Derived Catalysts. *Top. Catal.* **2003**, *22*, 305–318. [CrossRef]
12. Wang, G.-C.; Nakamura, J. Structure Sensitivity for Forward and Reverse Water-Gas Shift Reactions on Copper Surfaces: A DFT Study. *J. Phys. Chem. Lett.* **2010**, *1*, 3053–3057. [CrossRef]
13. Kim, S.S.; Lee, H.H.; Hong, S.C. A study on the effect of support's reducibility on the reverse water-gas shift reaction over Pt catalysts. *Appl. Catal. A Gen.* **2012**, *423–424*, 100–107. [CrossRef]
14. Kim, S.S.; Lee, H.H.; Hong, S.C. The effect of the morphological characteristics of TiO_2 supports on the reverse water–gas shift reaction over Pt/TiO_2 catalysts. *Appl. Catal. B Environ.* **2012**, *119–120*, 100–108. [CrossRef]
15. Kim, S.S.; Park, K.H.; Hong, S.C. A study of the selectivity of the reverse water–gas-shift reaction over Pt/TiO_2 catalysts. *Fuel Process. Technol.* **2013**, *108*, 47–54. [CrossRef]
16. Lu, B.; Kawamoto, K. Direct synthesis of highly loaded and well-dispersed NiO/SBA-15 for producer gas conversion. *RSC Adv.* **2012**, *2*, 6800–6805. [CrossRef]
17. Wang, L.; Zhang, S.; Liu, Y. Reverse water gas shift reaction over Co-precipitated Ni-CeO_2 catalysts. *J. Rare Earths* **2008**, *26*, 66–70. [CrossRef]
18. Wang, S.; Feng, K.; Zhang, D.; Yang, D.; Xiao, M.; Zhang, C.; He, L.; Yan, B.; Ozin, G.A.; Sun, W. Stable Cu Catalysts Supported by Two-dimensional SiO_2 with Strong Metal-Support Interaction. *Adv. Sci.* **2022**, *9*, e2104972. [CrossRef]

19. Tang, R.; Zhu, Z.; Li, C.; Xiao, M.; Wu, Z.; Zhang, D.; Zhang, C.; Xiao, Y.; Chu, M.; Genest, A.; et al. Ru-Catalyzed Reverse Water Gas Shift Reaction with Near-Unity Selectivity and Superior Stability. *ACS Mater. Lett.* **2021**, *3*, 1652–1659. [CrossRef]
20. Panaritis, C.; Edake, M.; Couillard, M.; Einakchi, R.; Baranova, E.A. Insight towards the role of ceria-based supports for reverse water gas shift reaction over RuFe nanoparticles. *J. CO2 Util.* **2018**, *26*, 350–358. [CrossRef]
21. Serrano-Lotina, A.; Daza, L. Long-term stability test of Ni-based catalyst in carbon dioxide reforming of methane. *Appl. Catal. A Gen.* **2014**, *474*, 107–113. [CrossRef]
22. Bian, L.; Wang, W.; Xia, R.; Li, Z. Ni-based catalyst derived from Ni/Al hydrotalcite-like compounds by the urea hydrolysis method for CO methanation. *RSC Adv.* **2016**, *6*, 677–686. [CrossRef]
23. Xu, C.; Chen, G.; Zhao, Y.; Liu, P.; Duan, X.; Gu, L.; Fu, G.; Yuan, Y.; Zheng, N. Interfacing with silica boosts the catalysis of copper. *Nat. Commun.* **2018**, *9*, 3367. [CrossRef] [PubMed]
24. Xin, J.; Cui, H.; Cheng, Z.; Zhou, Z. Bimetallic Ni-Co/SBA-15 catalysts prepared by urea co-precipitation for dry reforming of methane. *Appl. Catal. A Gen.* **2018**, *554*, 95–104. [CrossRef]
25. Chrouda, A.; Mahmoud Ali Ahmed, S.; Babiker Elamin, M. Preparation of Nanocatalysts Using Deposition Precipitation with Urea: Mechanism, Advantages and Results. *ChemBioEng Rev.* **2022**, *9*, 248–264. [CrossRef]
26. Guo, M.; Lu, G. The effect of impregnation strategy on structural characters and CO_2 methanation properties over MgO modified Ni/SiO_2 catalysts. *Catal. Commun.* **2014**, *54*, 55–60. [CrossRef]
27. Wang, F.; Han, B.; Zhang, L.; Xu, L.; Yu, H.; Shi, W. CO_2 reforming with methane over small-sized Ni@SiO_2 catalysts with unique features of sintering-free and low carbon. *Appl. Catal. B Environ.* **2018**, *235*, 26–35. [CrossRef]
28. Pu, T.; Shen, L.; Liu, X.; Cao, X.; Xu, J.; Wachs, I.E.; Zhu, M. Formation and influence of surface hydroxyls on product selectivity during CO_2 hydrogenation by Ni/SiO_2 catalysts. *J. Catal.* **2021**, *400*, 228–233. [CrossRef]
29. Gao, Z.; Li, C.; Shao, Y.; Gao, G.; Xu, Q.; Tian, H.; Zhang, S.; Hu, X. Sequence of Ni/SiO_2 and Cu/SiO_2 in dual catalyst bed significantly impacts coke properties in glycerol steam reforming. *Int. J. Hydrogen Energy* **2021**, *46*, 26367–26380. [CrossRef]
30. Wang, L.; Hu, R.; Liu, H.; Wei, Q.; Gong, D.; Mo, L.; Tao, H.; Zhang, Z. Encapsulated Ni@La2O3/SiO2 Catalyst with a One-Pot Method for the Dry Reforming of Methane. *Catalysts* **2020**, *10*, 38. [CrossRef]
31. Wang, L.; Liu, H.; Liu, Y.; Chen, Y.; Yang, S. Influence of preparation method on performance of Ni-CeO2 catalysts for reverse water-gas shift reaction. *J. Rare Earths* **2013**, *31*, 559–564. [CrossRef]
32. Cheng, H.; Li, G.; Zhao, H.; Lu, X.; Xu, Q.; Tao, W. Effects of preparation technique and lanthana doping on Ni/La_2O_3-ZrO_2 catalysts for hydrogen production by CO_2 reforming of coke oven gas. *Catal. Today* **2018**, *318*, 23–31. [CrossRef]
33. Zhang, Q.; Tang, T.; Wang, J.; Sun, M.; Wang, H.; Sun, H.; Ning, P. Facile template-free synthesis of Ni-SiO_2 catalyst with excellent sintering- and coking-resistance for dry reforming of methane. *Catal. Commun.* **2019**, *131*, 105782. [CrossRef]
34. Zhao, B.; Yao, Y.; Shi, H.; Yang, F.; Jia, X.; Liu, P.; Ma, X. Preparation of Ni/SiO_2 catalyst via novel plasma-induced micro-combustion method. *Catal. Today* **2019**, *337*, 28–36. [CrossRef]
35. Xu, Y.; Lin, Q.; Liu, B.; Jiang, F.; Xu, Y.; Liu, X. A Facile Fabrication of Supported Ni/SiO_2 Catalysts for Dry Reforming of Methane with Remarkably Enhanced Catalytic Performance. *Catalysts* **2019**, *9*, 183. [CrossRef]
36. Yang, M.; Jin, P.; Fan, Y.; Huang, C.; Zhang, N.; Weng, W.-z.; Chen, M.; Wan, H.-L. Ammonia-assisted synthesis towards a phyllosilicate-derived highly-dispersed and long-lived Ni/SiO_2 catalyst. *Catal. Sci. Technol.* **2015**, *5*, 5095–5099. [CrossRef]
37. Price, C.A.H.; Pastor-Perez, L.; Reina, T.R.; Liu, J. Yolk-Shell structured NiCo@SiO_2 nanoreactor for CO_2 upgrading via reverse water-gas shift reaction. *Catal. Today* **2022**, *383*, 358–367. [CrossRef]